Supporting Information

Efficient Screening of Metal Promoters of Pt Catalyst for C-H bond Activation in Propane Dehydrogenation from a Combined First-Principles Calculations and Machine Learning Study

Nuodan Zhou[a,b], Wen Liu[d], Faheem Jan[a,b] , ZhongKang Han[d]*, Bo Li[c*]

[a] Shenyang National Laboratory for Materials Science, Institute of Metal Research, Chinese Academy of Sciences, Shenyang 110016, Liaoning, People's Republic of China

[b] School of Materials Science and Engineering, University of Science and Technology of China, Shenyang 110016, Liaoning, People's Republic of China

[c] Institute of Catalysis for Energy and Environment, College of Chemistry and Chemical Engineering, Shenyang Normal University, Shenyang 110034, China

[d] School of Materials Science and Engineering, Zhejiang University, Hangzhou, 310027, China

Corresponding Author

* B. Li: boli@synu.edu.cn

*Z.K. Han: hanzk@zju.edu.cn

Note S1. Detail process of ML-DFT

(1) Data collection: The adsorption energy and reaction energy were calculated from DFT calculations. The complete adsorption energy data was listed in Table S1. CINEB was used to calculate the activation energy barrier of C-H bond, as shown in Table S2. The rest energy barrier values were obtained by BEP rules as shown in Figure S4. The complete reaction barriers are shown in Table S3.

(2) Data preprocessing: Normalized and preprocessed the DFT data we calculated. Scale the data so that it falls into small, specific intervals with the help of StandardScaler. Removed the unit restriction of data and converted into a dimensionless pure value, which is convenient for the comparison of indicators of different units and magnitudes.

(3) Feature engineering: Select 21 features that can describe the characteristics of the system as illustrated in Table S5, Pearson relation is used to get rid of the feature of high linear correlation coefficient as shown in Table S7

(4) Model construction: The input data collected from DFT computations were randomly shuffled and divided into the training set and test set with a 8:2 ratio. To reduce the risk of overfitting, the test data set is reproduced by adding uniformly distributed random noises in the scale of−2% to 2% of the test set, and the training procedure is executed 500 times for each ML model. Analyzed the train set of the preprocessed data by four ML regression algorithms including GBR, KNR, RFR, and ABR, select the model with the least error and the best performance.

(5) Model prediction : The optimal model selected is used for prediction, and the prediction results are shown in the Table S8.

Note S2. The calculated lattice constants

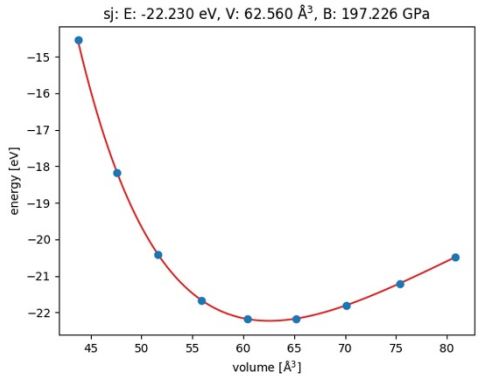	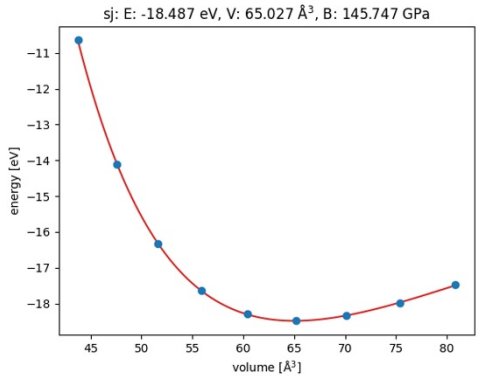
Pt: 3.97Å	Pt_3Sn: 4.02Å
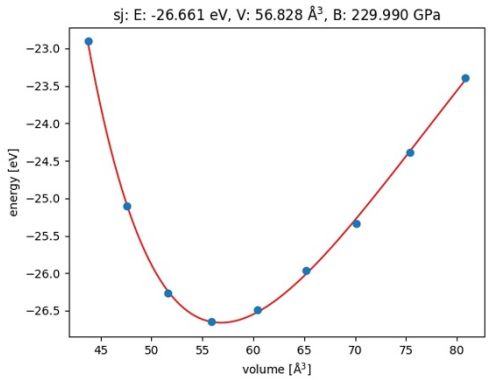	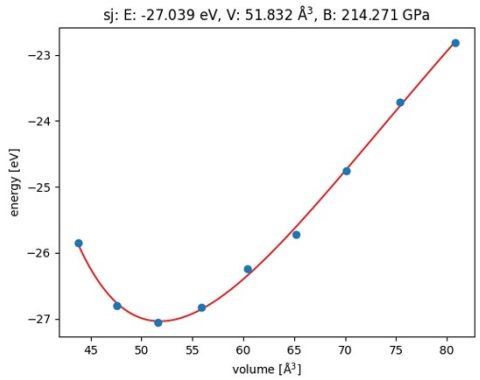
Pt_3Co: 3.84Å	PtCo: 3.73Å
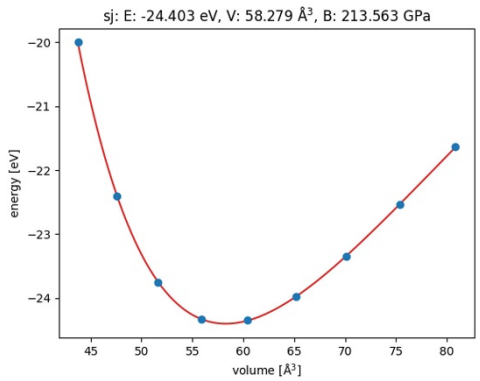	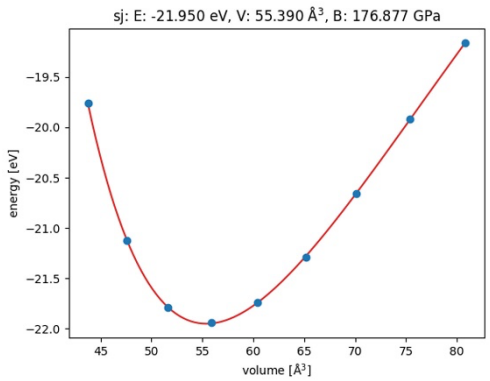
Pt_3Cu: 3.88Å	PtCu: 3.81Å

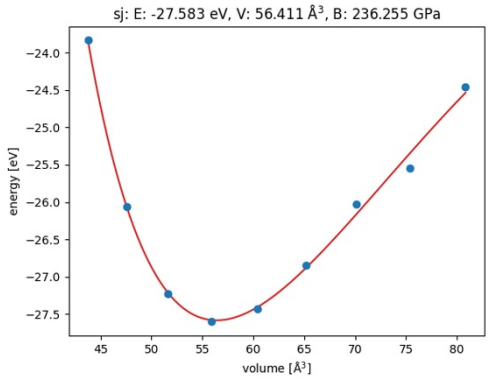	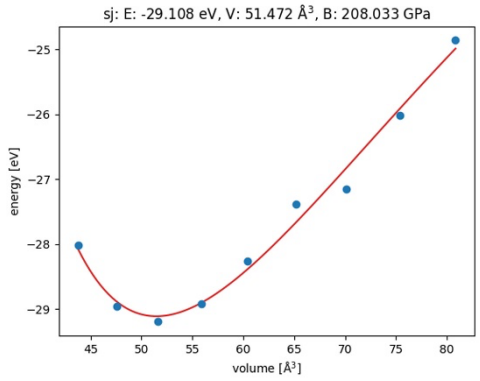
Pt_3Fe: 3.84Å	PtFe: 3.72Å
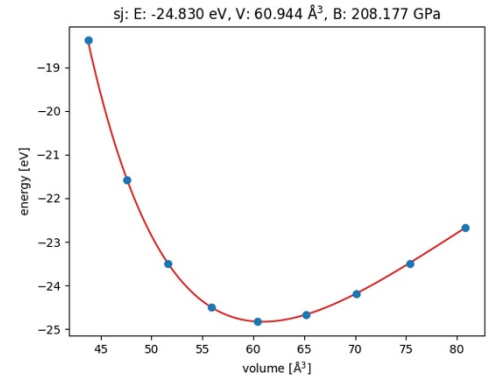	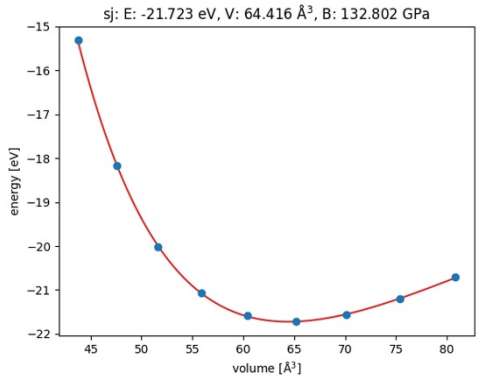
Pt_3Ge: 3.94Å	PtGe: 4.01Å
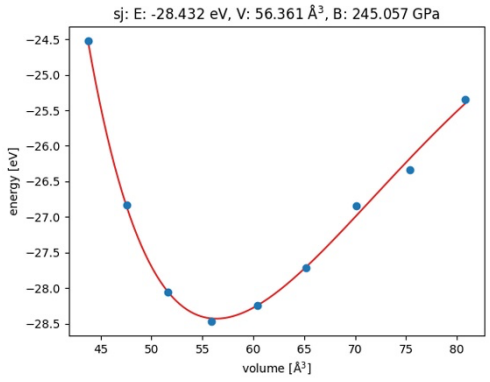	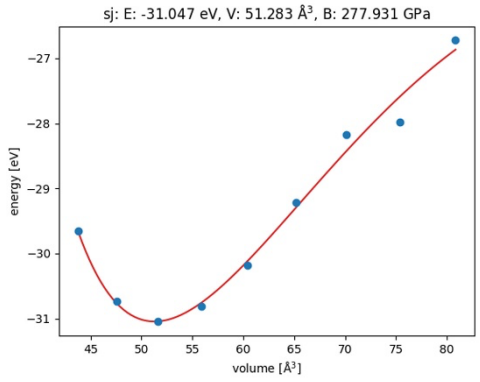
Pt_3Mn: 3.84Å	PtMn: 3.72Å
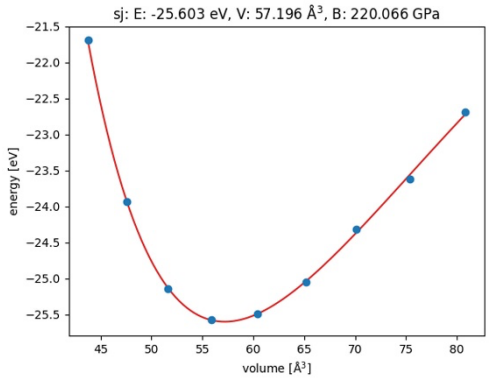	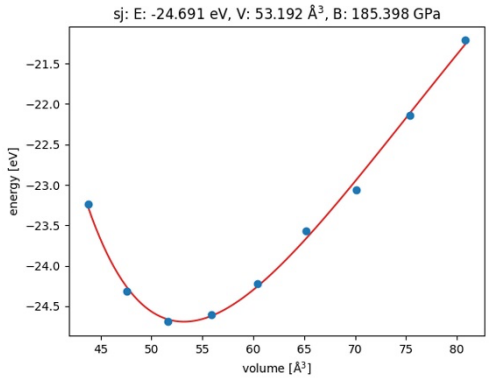
Pt_3Ni: 3.85Å	PtNi: 3.76Å

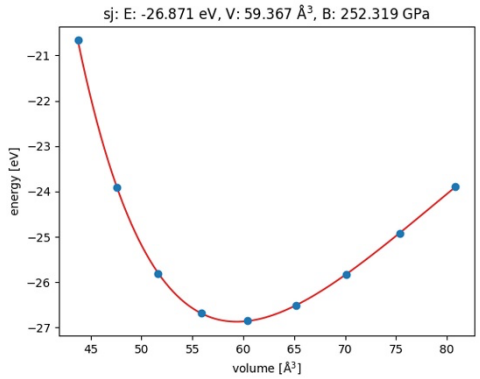	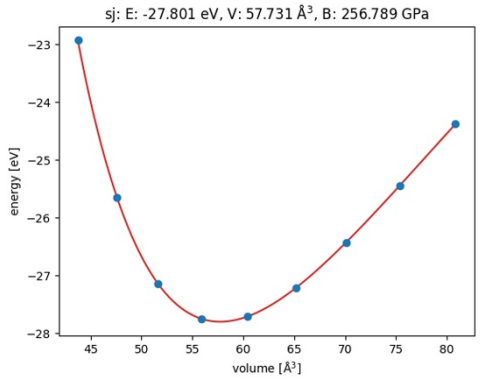
Pt_3Rh: 3.90Å	PtRh: 3.86Å
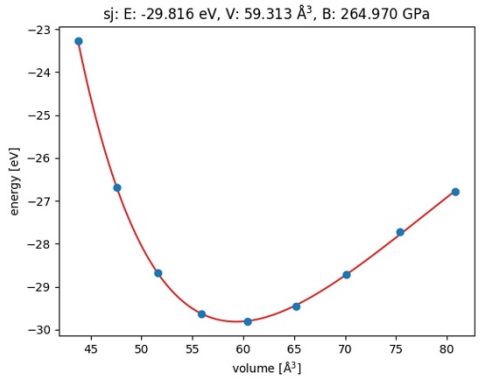	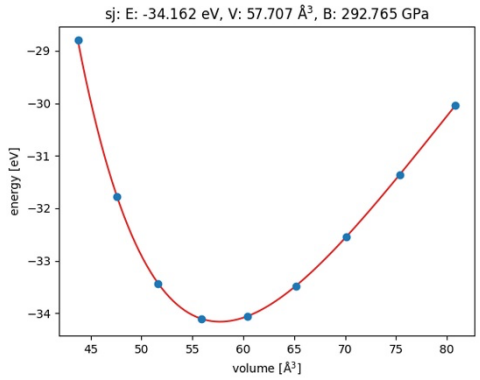
Pt_3Tc: 3.90Å	PtTc: 3.86Å
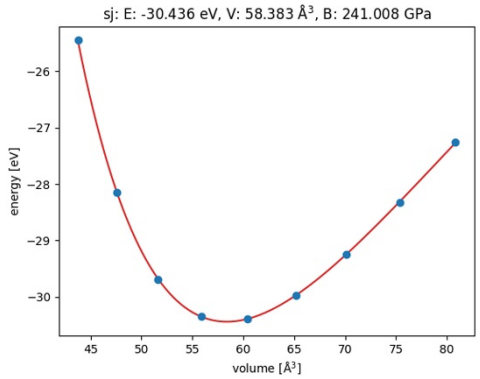	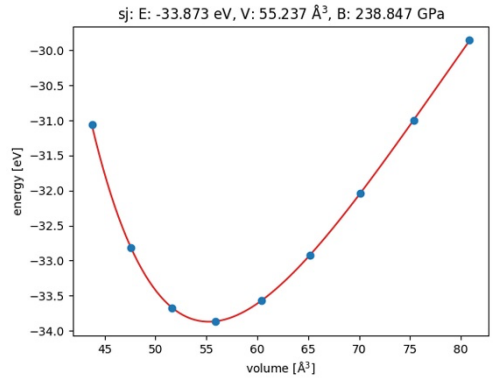
Pt_3V: 3.88Å	Pt_3V: 3.81Å

Note S3. The computational method of GBR regression algorithm

The best performing **Gradient Boosted Regression (GBR)** model is an integrated ML algorithm that is generated by the integration of weak regression trees. Given the training samples $\boldsymbol{D} = \{(\mathbf{x_1}, \mathbf{y_1}), (\mathbf{x_2}, \mathbf{y_2}) \ldots, (\mathbf{x_n}, \mathbf{y_n})\}$, the number of leaf nodes in every regression tree is **J**. We divided the input data into J disjoint areas and defined each regression tree as $\mathbf{t_m(x)}$. The training goal of GBR is to minimize the loss function **L**, and the parameters of decision tree $\boldsymbol{\theta_m}$ are determined through empirical risk

minimization:

$$\boldsymbol{\theta_m} = \underset{\boldsymbol{\theta_m}}{\boldsymbol{argmin}} \sum_{\boldsymbol{i=1}}^{\boldsymbol{n}} \boldsymbol{L}\left(\boldsymbol{y_i}, \boldsymbol{f_{(m-1)}(x_i)} + \boldsymbol{t_m(x_i)}\right) \quad (\boldsymbol{S1})$$

The process of GBR training is as follows:

(a) Initialize a regression tree function $f_0(x)$.

(b) Train GBR in the gradient decline direction, and compute the negative gradient value of the loss function as the estimated value of the residual. For the m_{th} iteration, GBR generates a regression tree according to the residual and updates the current function $f_m(x)$.

(c) The final regression model is the weighted sum of several weak regression trees, which is defined as:-

$$\boldsymbol{f_M(x)} = \sum_{\boldsymbol{m=1}}^{\boldsymbol{M}} \boldsymbol{t(x, \theta_m)} \quad (\boldsymbol{S2})$$

Note S4. The computational method of RFR regression algorithm

The Random Forest Regression (RFR) model are an ensemble learning method for regression by constructing a multitude of decision trees at training time and outputting the class that is the mode of the classes (classification) or mean/average prediction (regression) of the individual trees. Random decision forests correct for decision trees' habit of overfitting to their training set. The training algorithm for random forests applies the general technique of bootstrap aggregating, or bagging, to tree learners. Given a training set $X = x_1 \ldots x_n$ with responses $Y = y_1 \ldots y_n$, bagging repeatedly (B times) selects a random sample with replacement of the training set and fits trees to these samples:

(a) For b = 1... B: Sample, with replacement, n training examples from X, Y; call these X_b, Y_b; Train a regression tree f_b on X_b, Y_b.

(b) After training, predictions for unseen samples x' can be made by averaging the predictions from all the individual regression trees on x'

$$\hat{\boldsymbol{f}} = \frac{\boldsymbol{1}}{\boldsymbol{B}} \sum_{\boldsymbol{b=1}}^{\boldsymbol{B}} \boldsymbol{f_b(x')} \quad (\boldsymbol{S3})$$

Note S5. The computational method of KNR regression algorithm

The **K-Neighbor Regression (KNR)** model is a non-parametric method proposed by Thomas Cover used for classification and regression. In both cases, the input consists of the k closest training examples in the feature space. The output depends on whether k-NN is used for classification or regression. In k-NN regression, the output is the property value for the object. This value is the average of the values of k nearest neighbors.In the classification phase, k is a user-defined constant, and an unlabeled vector (a query or test point) is classified by assigning the label which is most frequent among the k training samples nearest to that query point. A commonly used distance metric for continuous variables is Euclidean distance. For discrete variables, such as for text classification, another metric can be used, such as the overlap metric (or Hamming distance). Often, the classification accuracy of k-NN can be improved significantly if the distance metric is learned with specialized algorithms such as Large Margin Nearest Neighbor or Neighborhood components analysis. This algorithm works as follows:

(a) Compute the Euclidean or Mahalanobis distance from the query example to the labeled examples.

(b) Order the labeled examples by increasing distance.

(c) Find a heuristically optimal number k of nearest neighbors, based on RMSE. This is done using cross validation.

(d) Calculate an inverse distance weighted average with the k-nearest multivariate neighbors

Note S6. The computational method of ABR regression algorithm

In each iteration, the weight of the data misclassified by the previous classifier is improved, while the weight of the data correctly classified is reduced. Finally, AdaBoost takes the linear combination of basic classifiers as a strong classifier, in which the basic classifier with a small classification error rate is given large weights and the basic classifier with large classification error rate is given small weights. M means that the lifting tree has M weak classifiers. $G_m(x)$ denotes the mth weak classifier, and α_m is the parameter of the Mth weak classifier. $w_{i,m}$ represents the weight of the i instance around m. The algorithmic principle of AdaBoost is as follow:

(a) Entering training data D = $\{(x_1,y_1),\ldots,(x_m,y_m)\}$, which x_m is feature vector, y_m is target vector, and m is the number of training data

(b) Initialize the weight vector by the following equation:

$$w_1(x_i) = \frac{1}{m} \qquad S4$$

(c) Finding T weak learners h_t(t=1,2,…,T) and initialization t =0
Determine $P_t(x_i)$

$$P_t(x_i) = \frac{w_t(x_i)}{\sum_{i=1}^{m} w_t(x_i)} \quad S5$$

Calculate the error rate:

$$\varepsilon_t = \sum P_t(x_i)[h_t(x_i) - y_i] \quad S6$$

If $\varepsilon_t > 0.5$ and T = t-1 exit the loop

Calculate weight confidence α_t

$$\alpha_t = \log \frac{\varepsilon_t}{1 - \varepsilon_t} \quad S7$$

Modify the weight of all training data from i to m:

$$w_{t+1}(x_i) = w_t(x_i) \times e^{-y_i h_t(x_i) \alpha_t} \quad S8$$

If $\varepsilon_t > 0.001$ and $t < T$ return to A

$$w_{t+1}(x_i) = w_t(x_i) \times e^{-y_i h_t(x_i) \alpha_t} \quad S9$$

(d) The output is a strong learner that combines weak weight learners:

$$H(x) = sign\left[\sum_{t}^{T} \alpha_t [h_t(x) = y]\right] \quad S10$$

Note S7. The computational methods of R^2 score and RMSE

The prediction accuracy of ML models is evaluated with R^2 score and RMSE, which are expressed as:

$$R^2 = 1 - \frac{\frac{1}{n}\sum_{i=1}^{n}(y_i - \dot{y}_i)^2}{\frac{1}{n}\sum_{i=1}^{n}(y_i - \gamma_i)^2} \quad S11$$

$$RMSE = \sqrt{\frac{1}{n}\sum_{i=1}^{n}(y_i - \dot{y}_i)^2} \quad S12$$

where y_i indicates the ground truth and y_i indicates the prediction of the model. R^2 score ranges from 0 to 1, and the closer it is to 1, the better the prediction performance of the model is. RMSE represents the loss between the prediction and the ground truth. The loss is lower, the model performs better.

Note S8. The computational methods of Leave-One-Out Cross-Validation (LOOCV)

LOOCV provides train/test indices to split data in train/test sets. Each sample is used once as a test set (singleton) while the remaining samples form the training set. LOOCV estimate of test error is averaged over the n models:

$$CV_n = \frac{1}{n}\sum_{i=1}^{n}(y_i - \hat{y}_i)^2 \quad S13$$

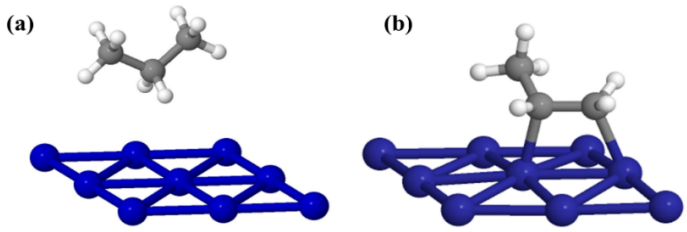

Figure S1. The adsorption configurations of (a) propane and (b) propene

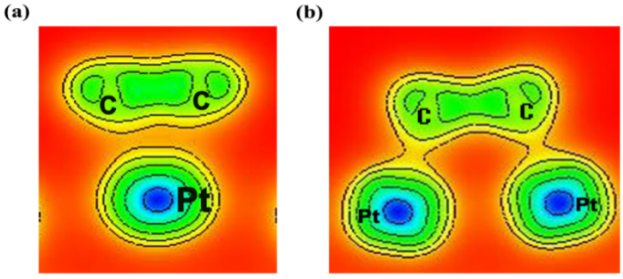

Figure S2. The ELF diagrams of (a) propane adsorption and (b) propene adsorption

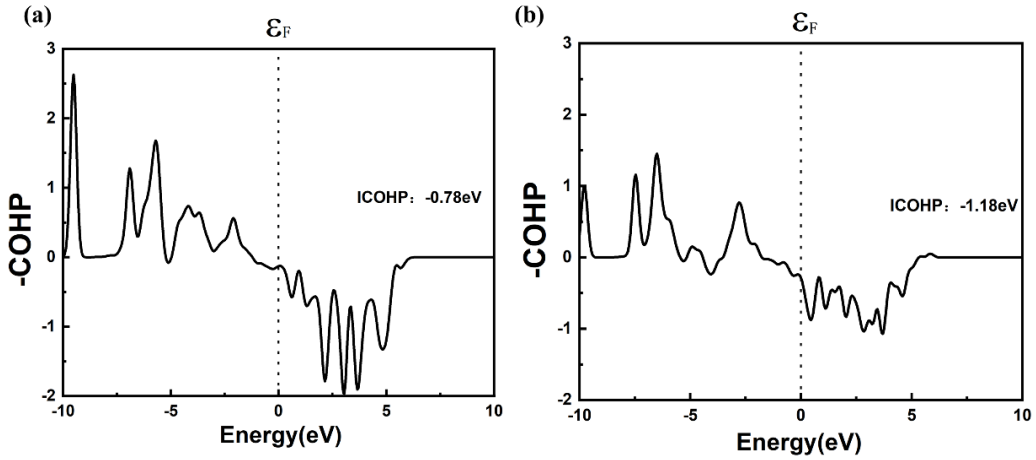

Figure S3. The COHP diagrams of (a) propane adsorption and (b) propene adsorption

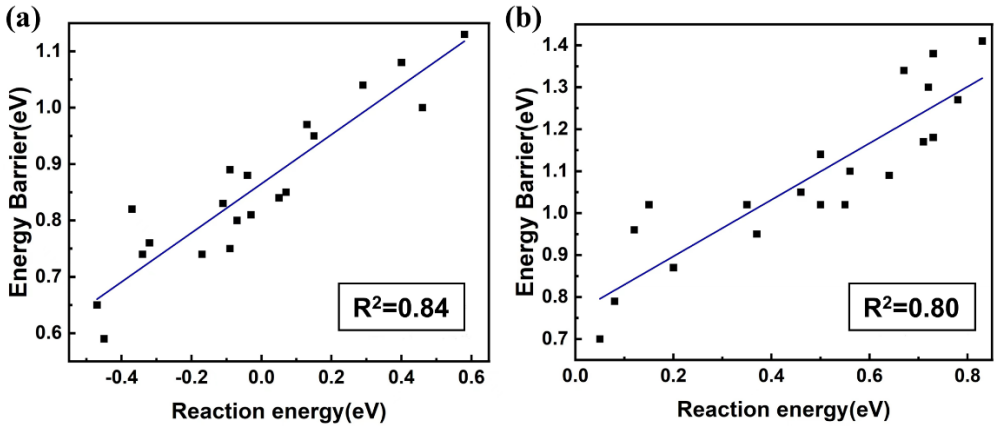

Figure S4. BEP relation of energy barriers and reaction energy of the C-H bond breaking of (a) propane (b) propene

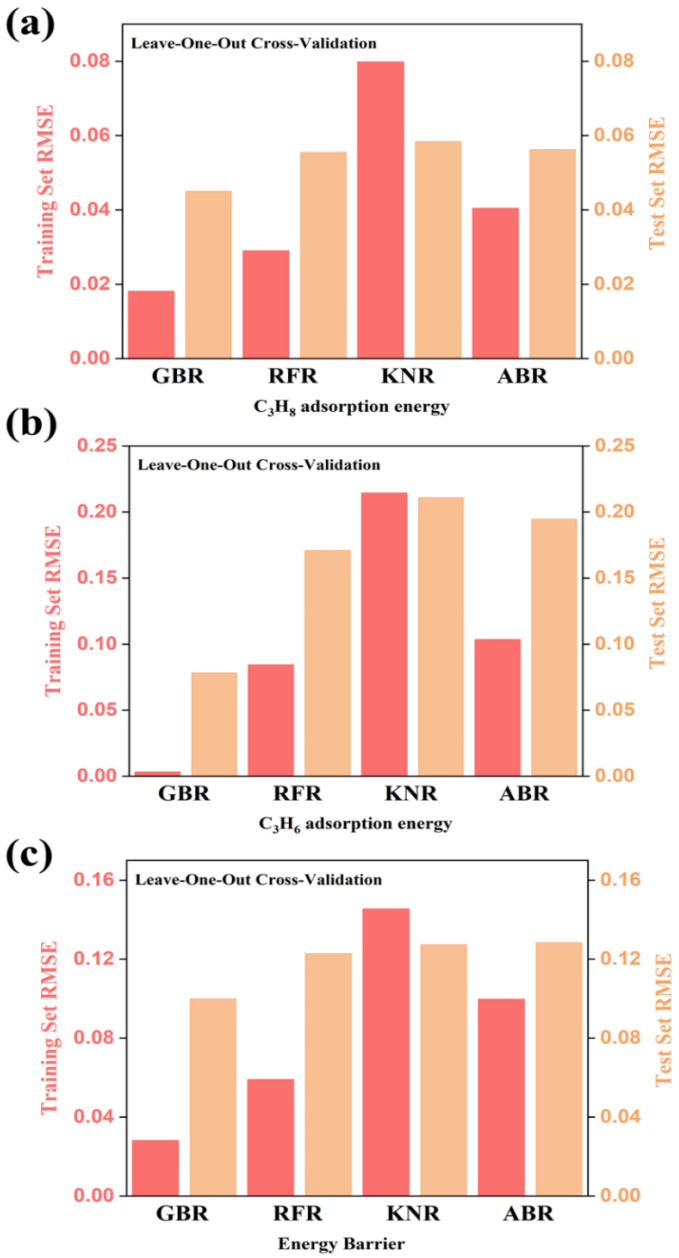

Figure S5. Leave-One-Out Cross-Validation average RMSE of (a) Propane adsorption energy (b) Propene adsorption energy (c) Energy barrier of C-H bond breaking

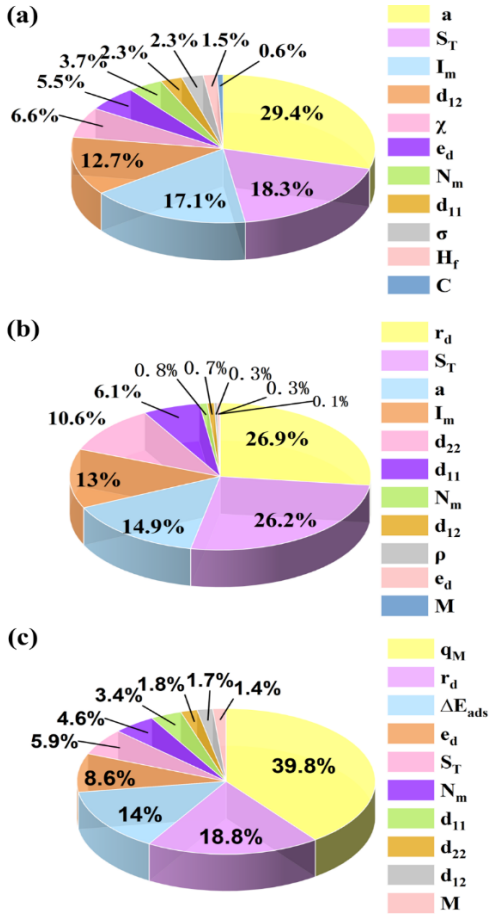

Figure S6. Feature importance of (a) Propane adsorption energy (b) Propene adsorption energy (c) Energy barrier of C-H bond breaking.

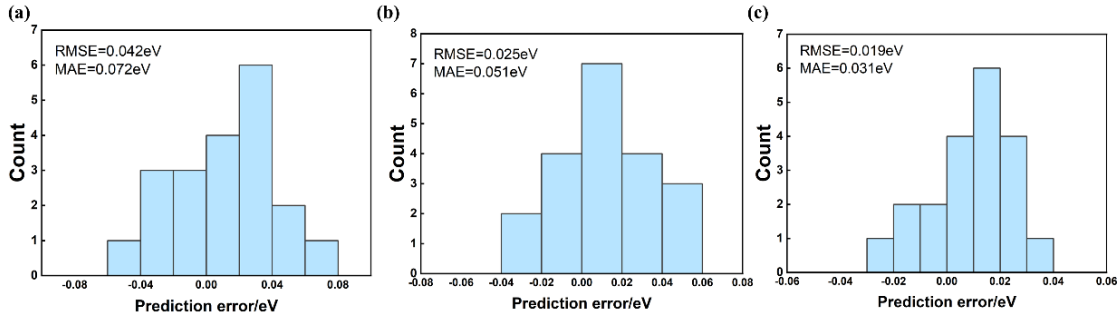

Figure S7. The error distributions for all the lower-dimensional models of E_{b8}: (a) 1D, (b) 2D, (c) 3D.

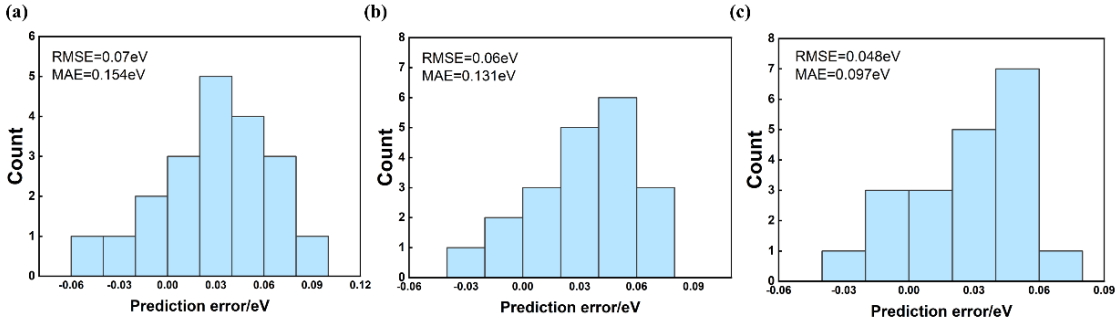

Figure S8. The error distributions for all the lower-dimensional models of E_{b6}: (a) 1D, (b) 2D, (c) 3D.

Table S1. Summary of adsorption energy in literature and current work.

Propane adsorption(eV)			Propene adsorption(eV)		
	Current work	literature		Current work	literature
Pt_3Sn/Pt	-0.43	-0.34 [1]	Pt	-1.79	-1.68 [2]
Pt_3Sn/Pt	-0.43	-0.41 [3]	Pt	-1.79	-1.41 [4]
Pt_3Sn	-0.36	-0.33 [1]	Pt_3In	-1.29	-1.31 [4]
Pt_3Sn	-0.36	-0.38 [3]	PtRu	-1.00	-0.95 [4]
Pt	-0.51	-0.35 [2]			
Pt	-0.51	-0.46 [4]			
Pt	-0.51	-0.42 [3]			
PtRu	-0.51	-0.44 [4]			

Table S2. Summary of energy barrier in literature and current work.

Energy barriers for propane dehydrogenation(eV)			Energy barriers for propylene deep dehydrogenation(eV)		
	Current work	literature		Current work	literature
Pt_3Sn	0.85	0.78 [3]	Pt_3Sn	1.05	1.11 [3]
Pt	0.76	0.77 [2]	Pt	1.02	1.08 [2]
Pt	0.76	0.70 [3]	Pt	1.02	0.77 [3]
PtNi	0.65	0.62 [4]	Pt_3V	0.96	1.02 [5]
PtRu	0.59	0.63 [4]	Pt_3Ga	1.09	1.3 [5]
			Pt_3In	0.87	0.86 [5]

Table S3. Summary of lattice constants in literature and current work.

	Current work	literature
Pt	3.97	4.04Å [1]
Pt	3.97	3.93Å [6]
Pt	3.97	3.98Å [7]
Pt_3Sn	4.02	4.10Å [1]
Pt_3Sn	4.02	4.00Å [6]

Table S4. Summary of applied method, descriptor, PtM model, predicted best candidate in literature and current work.

Ref 1 [8]	
Method	Descriptor screening
Descriptor	CH_3 and CH binding energy

PtM model	First layer surface adding
Best catalyst	High coverage: Pt_3Pb, Low overage: PtSb
	Ref 2 [9]
Method	Descriptor based microkinetic
Descriptor	CH_3 and CH binding energy
PtM model	Bulk adding
Best catalyst	Pt_3Ga
	Ref 3 [10]
Method	Descriptor based microkinetic
Descriptor	formation energy of CH_3CH_2* and CH*
PtM model	Bulk adding
Best catalyst	NiMo
	Current work
Method	Machine learning
Descriptor	C-H bond activation energy and propene adsorption
PtM model	Bulk adding, first layer surface adding, and sub-layer surface adding
Best catalyst	Pt_3Mo

Table S5. Adsorption energy of propane and propylene on Pt-M obtained from DFT calculations.

Configuration of PtM(111)	Adsorption energy of propane(eV)	Adsorption energy of propylene (eV)
Pt	-0.510	-1.790
Sn-firstlayer-3:1	-0.432	-1.219
Sn-bulk-3:1	-0.357	-1.022
Sn-secondlayer-1:1	-0.557	-1.580
Zn-bulk-3:1	-0.566	-1.062
Zn-bulk-1:1	-0.473	-0.989
Zn-firstlayer-3:1	-0.537	-1.584
Zn-secondlayer-3:1	-0.596	-1.607
In-bulk-3:1	-0.501	-1.287
In-secondlayer-3:1	-0.595	-1.442
In-firstlayer-3:1	-0.447	-1.139
In-secondlayer-1:1	-0.597	-1.234
Ga-secondlayer-3:1	-0.595	-1.844
Ga-firstlayer-1:1	-0.678	-1.426
Ga-firstlayer-3:1	-0.676	-1.697
Ga-secondlayer-1:1	-0.628	-1.758
Cu-bulk-3:1	-0.584	-1.533
Cu-firstlayer-3:1	-0.568	-1.821
Cu-bulk-1:1	-0.619	-1.493

Cu-secondlayer-3:1	-0.648	-1.672
Cu-firstlayer-1:1	-0.604	-1.504
Cu-secondlayer-1:1	-0.602	-1.571
Ag-bulk-3:1	-0.553	-1.270
Ag-firstlayer-3:1	-0.567	-1.253
Ag-bulk-1:1	-0.562	-1.972
Ge-bulk-3:1	-0.465	-1.734
Ge-secondlayer-3:1	-0.579	-1.391
Ni-bulk-3:1	-0.731	-1.992
Ni-bulk-1:1	-0.532	-1.564
Ni-firstlayer-3:1	-0.713	-2.316
Ni-secondlayer-3:1	-0.593	-1.150
Ni-secondlayer-1:1	-0.597	-1.677
Co-bulk-1:1	-0.495	-1.610
Co-firstlayer-3:1	-0.535	-1.377
Co-secondlayer-3:1	-0.594	-0.189
Co-firstlayer-1:1	-0.502	-1.623
Co-secondlayer-1:1	-0.575	-1.622
Fe-firstlayer-3:1	-0.580	-1.397
Au-bulk-3:1	-0.600	-0.650
Au-firstlayer-3:1	-0.577	-0.927
Au-bulk-1:1	-0.583	-1.607
Nb-bulk-3:1	-0.497	-0.887
Nb-bulk-1:1	-0.472	-0.551
Nb-firstlayer-3:1	-0.531	-1.589
Nb-secondlayer-3:1	-0.587	-1.777
Mo-bulk-1:1	-0.476	-1.422
Mo-firstlayer-3:1	-0.668	-1.184
Ru-firstlayer-3:1	-0.539	-1.531
Ru-bulk-3:1	-0.542	-1.734
Ru-bulk-1:1	-0.511	-1.009
Ru-secondlayer-3-1	-0.589	-1.972
Ti-firstlayer-3:1	-0.656	-1.471
Ti-bulk-3:1	-0.548	-1.659
Ti-bulk-1:1	-0.739	-1.576
Ti-secondlayer-3:1	-0.592	-1.779
Pd-bulk-3:1	-0.589	-1.587
Pd-bulk-1:1	-0.586	-0.716
Pd-firstlayer-3:1	-0.597	-0.909
Cr-secondlayer-3:1	-0.586	-1.170
Tl-firstlayer-3:1	-0.389	-1.058
Hg-firstlayer-3:1	-0.504	-1.166
Hg-bulk-3:1	-0.520	-0.973
Cd-bulk-3:1	-0.503	-1.006

Cd-bulk-1:1	-0.448	-1.234
Cd-firstlayer-3:1	-0.507	-0.793
Pb-bulk-3:1	-0.442	-0.579
Pb-firstlayer-3:1	-0.346	-1.075
V-bulk-3:1	-0.514	-1.336
V-bulk-1:1	-0.507	-1.738
V-secondlayer-3:1	-0.594	-1.512
V-firstlayer-1:1	-0.507	-1.694
V-secondlayer-1:1	-0.633	-1.216
Tc-bulk-3:1	-0.499	-1.235
Tc-firstlayer-3:1	-0.514	-1.683

Table S6. The C-H bond activation energy barrier and reaction energy of Pt-M calculated from DFT calculation.

	Propane to 2-propyl		Propene to 2-propenyl	
Promoter element	Reaction Energy(eV)	Energy Barrier(eV)	Reaction Energy(eV)	Energy Barrier(eV)
Ga	-0.07	0.80	0.37	0.95
Co	0.46	1.00	0.50	1.02
V	-0.04	0.88	0.12	0.96
Cu	0.05	0.84	0.83	1.41
Zn	0.40	1.08	0.56	1.10
Ag	-0.11	0.83	0.50	1.14
Ru	-0.03	0.81	0.08	0.79
Pd	-0.09	0.75	0.35	1.02
Au	-0.17	0.74	0.73	1.18
Sn	0.07	0.85	0.46	1.05
Nb	0.29	1.04	0.64	1.09
Tc	0.13	0.97	0.72	1.30
Sc	-0.37	0.82	0.71	1.17
Ni	-0.47	0.65	0.67	1.34
Ru	-0.45	0.59	0.78	1.27
Ti	-0.34	0.74	0.05	0.70
Rh	0.58	1.13	0.73	1.38
Hg	0.15	0.95	0.55	1.22
Pt	-0.32	0.76	0.15	1.02
In	-0.09	0.89	0.20	0.87

Table S7. The C-H bond activation energy barrier of propane and propylene on Pt-M obtained from BEP relations shown in Figure S4.

Configuration of PtM(111)	Energy barrier of Propane to 2-propyl(eV)	Energy barrier of Propene to 2 propenyl(eV)
Pt	0.760	1.020
Sn-firstlayer-3:1	0.852	1.386
Sn-bulk-3:1	0.893	1.048
Sn-firstlayer-1:1	0.997	1.332
Sn-secondlayer-1:1	0.964	1.217
Zn-bulk-3:1	0.965	1.234
Zn-bulk-1:1	1.056	1.116
Zn-firstlayer-3:1	0.713	1.115
Zn-secondlayer-3:1	0.672	1.014
In-bulk-3:1	0.919	1.257
In-secondlayer-3:1	0.811	0.725
In-firstlayer-3:1	0.916	0.868
In-firstlayer-1:1	0.999	1.217
In-secondlayer-1:1	1.065	1.075
Ga-bulk-3:1	0.715	1.016
Ga-secondlayer-3:1	0.830	0.741
Ga-firstlayer-1:1	0.793	0.892
Ga-firstlayer-3:1	0.753	1.158
Ga-secondlayer-1:1	0.960	0.994
Cu-bulk-3:1	0.879	1.307
Cu-firstlayer-3:1	0.640	1.064
Cu-bulk-1:1	0.863	1.080
Cu-secondlayer-3:1	0.763	0.954
Cu-firstlayer-1:1	0.637	1.115
Cu-secondlayer-1:1	0.913	0.736
Ag-bulk-3:1	0.802	1.204
Ag-firstlayer-3:1	0.801	1.075
Ag-bulk-1:1	0.954	1.192
Ge-bulk-3:1	0.827	0.894
Ge-secondlayer-3:1	0.611	0.786
Ni-bulk-3:1	0.825	1.027
Ni-bulk-1:1	0.854	0.988
Ni-firstlayer-3:1	0.627	1.102
Ni-secondlayer-3:1	0.760	0.871
Ni-secondlayer-1:1	0.898	1.224
Ni-firstlayer-1:1	0.891	1.241
Co-bulk-1:1	1.084	1.075
Co-firstlayer-3:1	0.645	0.770
Co-secondlayer-3:1	0.790	1.015

Co-firstlayer-1:1	0.634	1.222
Co-secondlayer-1:1	0.957	1.064
Fe-firstlayer-3:1	0.628	1.056
Au-bulk-3:1	0.791	0.831
Au-firstlayer-3:1	0.773	1.134
Au-bulk-1:1	0.884	1.237
Nb-bulk-3:1	1.098	0.852
Nb-bulk-1:1	0.954	0.488
Nb-firstlayer-3:1	0.674	1.174
Nb-secondlayer-3:1	1.001	1.231
Mo-bulk-1:1	0.754	1.199
Mo-bulk-3:1	0.933	0.590
Ru-firstlayer-3:1	0.741	0.736
Ru-bulk-3:1	0.828	0.787
Ru-bulk-1:1	0.928	1.266
Ru-secondlayer-3-1	0.841	0.850
Ti-firstlayer-3:1	0.690	1.125
Ti-bulk-3:1	0.944	1.457
Ti-bulk-1:1	0.659	0.946
Ti-secondlayer-3:1	0.852	1.176
Pd-bulk-3:1	0.790	0.922
Pd-bulk-1:1	0.810	0.975
Pd-firstlayer-3:1	0.757	0.900
Cr-secondlayer-3:1	0.794	1.058
Cd-bulk-3:1	0.863	1.199
Pb-firstlayer-3:1	0.837	1.243
V-bulk-3:1	0.981	1.316
V-bulk-1:1	0.753	0.876
V-firstlayer-3:1	0.693	1.215
V-secondlayer-3:1	0.836	1.117
V-firstlayer-1:1	0.553	1.008
V-secondlayer-1:1	0.693	1.265
Tc-bulk-3:1	0.920	0.794
Tc-bulk-1:1	1.036	1.116
Tc-firstlayer-3:1	0.689	0.853
Tc-bulk-3:1	-0.499	-1.235
Tc-firstlayer-3:1	-0.514	-1.683

Table S8. The tabulated data shown in Figure 2.

Vertical axis	Horizontal axis (E_{Pt-M} minus E_{Pt})			
Pt-M configuration corresponding to each bar from the bottom up	Propane adsorption energy	C-H bond activation energy barrier of propane	Propene adsorption energy	C-H bond activation energy barrier of propene
Sn-firstlayer-3:1	0.078	0.571	0.092	0.366
Sn-bulk-3:1	0.153	0.768	0.133	0.028
Sn-secondlayer-1:1	-0.047	0.21	0.237	0.312
Zn-bulk-3:1	-0.056	0.728	0.204	0.197
Zn-bulk-1:1	0.037	0.801	0.205	0.214
Zn-firstlayer-3:1	-0.027	0.206	0.296	0.096
Zn-secondlayer-3:1	-0.086	0.183	-0.047	0.095
In-bulk-3:1	0.009	0.503	-0.088	-0.006
In-secondlayer-3:1	-0.085	0.348	0.159	0.237
In-firstlayer-3:1	0.063	0.651	0.051	-0.295
In-secondlayer-1:1	-0.087	0.556	0.156	-0.152
Ga-secondlayer-3:1	-0.085	-0.054	0.239	0.197
Ga-firstlayer-1:1	-0.168	0.364	0.305	0.055
Ga-firstlayer-3:1	-0.166	0.093	-0.045	-0.004
Ga-secondlayer-1:1	-0.118	0.032	0.07	-0.279
Cu-bulk-3:1	-0.074	0.257	0.033	-0.128
Cu-firstlayer-3:1	-0.058	-0.031	-0.007	0.138
Cu-bulk-1:1	-0.109	0.297	0.2	-0.026
Cu-secondlayer-3:1	-0.138	0.118	0.119	0.287
Cu-firstlayer-1:1	-0.094	0.286	-0.12	0.044
Cu-secondlayer-1:1	-0.092	0.219	0.103	0.06
Ag-bulk-3:1	-0.043	0.52	0.003	-0.066
Ag-firstlayer-3:1	-0.057	0.537	-0.123	0.095
Ag-bulk-1:1	-0.052	-0.182	0.153	-0.284
Ge-bulk-3:1	0.045	0.056	0.042	0.184
Ge-secondlayer-3:1	-0.069	0.399	0.041	0.055
Ni-bulk-3:1	-0.221	-0.202	0.194	0.172
Ni-bulk-1:1	-0.022	0.226	0.067	-0.126
Ni-firstlayer-3:1	-0.203	-0.526	-0.149	-0.234
Ni-secondlayer-3:1	-0.083	0.64	0.065	0.007
Ni-secondlayer-1:1	-0.087	0.113	0.094	-0.032
Co-bulk-1:1	0.015	0.18	-0.133	0.082
Co-firstlayer-3:1	-0.025	0.413	0	-0.149
Co-secondlayer-3:1	-0.084	1.601	0.138	0.204
Co-firstlayer-1:1	0.008	0.167	0.131	0.221
Co-secondlayer-1:1	-0.065	0.168	0.324	0.055
Fe-firstlayer-3:1	-0.07	0.393	-0.115	-0.25
Au-bulk-3:1	-0.09	1.14	0.03	-0.005

Au-firstlayer-3:1	-0.067	0.863	-0.126	0.202
Au-bulk-1:1	-0.073	0.183	0.197	0.044
Nb-bulk-3:1	0.013	0.903	-0.132	0.036
Nb-bulk-1:1	0.038	1.239	0.031	-0.189
Nb-firstlayer-3:1	-0.021	0.201	0.013	0.114
Nb-secondlayer-3:1	-0.077	0.013	0.124	0.217
Mo-bulk-1:1	0.034	0.368	0.338	-0.168
Mo-firstlayer-3:1	-0.158	0.606	0.194	-0.532
Ru-firstlayer-3:1	-0.029	0.259	-0.086	0.154
Ru-bulk-3:1	-0.032	0.056	0.241	0.211
Ru-bulk-1:1	-0.001	0.781	-0.006	0.179
Ru-secondlayer-3-1	-0.079	-0.182	0.173	-0.43
Ti-firstlayer-3:1	-0.146	0.319	-0.019	-0.284
Ti-bulk-3:1	-0.038	0.131	0.068	-0.233
Ti-bulk-1:1	-0.229	0.214	0.168	0.246
Ti-secondlayer-3:1	-0.082	0.011	0.081	-0.17
Pd-bulk-3:1	-0.079	0.203	-0.07	0.105
Pd-bulk-1:1	-0.076	1.074	0.184	0.437
Pd-firstlayer-3:1	-0.087	0.881	0.09	-0.074
Cr-secondlayer-3:1	-0.076	0.62	0.101	0.156
Tl-firstlayer-3:1	0.121	0.732	0.092	-0.098
Hg-firstlayer-3:1	0.006	0.624	0.03	-0.045
Hg-bulk-3:1	-0.01	0.817	-0.069	-0.12
Cd-bulk-3:1	0.007	0.784	0.05	0.038
Cd-bulk-1:1	0.062	0.556	-0.075	0.179
Cd-firstlayer-3:1	0.003	0.997	0.034	0.223
Pb-bulk-3:1	0.068	1.211	0.103	0.212
Pb-firstlayer-3:1	0.164	0.715	0.077	0.296
V-bulk-3:1	-0.004	0.454	0.221	-0.144
V-bulk-1:1	0.003	0.052	-0.007	0.195
V-secondlayer-3:1	-0.084	0.278	-0.067	0.097
V-firstlayer-1:1	0.003	0.096	0.067	-0.012
V-secondlayer-1:1	-0.123	0.574	0.16	0.245
Tc-bulk-3:1	0.011	0.555	0.276	-0.226
Tc-firstlayer-3:1	-0.004	0.107	-0.071	-0.167

Table S9. List of features for ML method

Atomic structures	group numbers	G
	period numbers	P
	relative atomic mass	M
	atomic radius	r_d
	lattice parameter	a
Physical	the standard heat of formation	H_f

properties	the standard molar entropy	$S°$
	density	ρ
	specific heat capacity	C
	melting point	M_p
	electrical conductance	σ
Description of electronic structure	electron affinity	χ
	d electron count	e_d
	Pauli electronegativity	N_m
	the first ionization energy	I_m
Representation of alloy surface	second metal doping method	S_T
	bond length between metal atom and the nearest metal of monolayer	d_{11}
	bond length between metal atom and the nearest metal of second layer	d_{22}
	bond length of the layer spacing between the first and second layers	d_{12}
	Energy of optimized Pt/M(111)	ΔE
	Bader charge transfer of Pt atoms and C atoms	q_M

Table S10. parameters of ML model

Method	Parameter
GBR	Number of estimators: 400
	max depth: 6
	learning rate: 0.06
	loss function: Huber.
KNR	Number of neighbors: 5
	weights function: uniform
	distance metric: minkowski;
	Leaf size: 30
RFR	Number of estimators: 900
	criterion: mse
	mtry:7
ABR	Number of estimators: 800
	Learning rate: 0.1
SISSO	desc-dim: 5
	subs−sis: 50
	dimclass: (1:6)(7:9)(10:11)(12:12)(13:13)
	opset:(+)(-)(*)(/)(exp)(exp-)(^1)(^2)(^3)(sqrt)(cbrt)(log)(|-|)

Table S11. Atomic parameters as inputs in the ML model

Element	S°	χ	ed	Nm	Im
Ru	186.5	1.05	7	2.2	7.5
Hg	175	0	10	1.9	10.39
Nb	186.3	0.892	4	1.41	6.77
Ni	182.2	1.16	8	1.91	7.61
Cu	166.4	1.227	10	1.9	7.69
Mo	182	0.745	5	1.47	7.35
Ti	180.3	0.079	2	1.38	6.81
Pb	175.4	0.364	10	1.8	7.38
Ge	167.9	1.23	10	2.01	7.85
Co	179.5	0.66	7	1.88	7.81
Au	180.5	2.309	10	2.54	9.19
Cd	167.7	0	10	1.69	8.95
Fe	180.5	0.163	6	1.83	7.83
Sn	168.5	1.112	10	1.96	7.37
Tc	181.1	0.55	5	1.9	7.28
Pd	167.1	0.557	8	1.58	8.3
V	182.3	0.524	3	1.63	6.76
Ag	173	1.302	10	1.93	7.54
Zn	161	0	10	1.65	9.35
Cr	174.5	0.666	5	1.66	6.74
rd	M	ρ	C	σ	a
134	101.07	12.41	238	1.4	2.706
151	200.59	13.55	139.5	0.1	3.464
146	92.906	8.58	265	0.67	3.301
124	58.6934	8.902	445	1.4	3.524
128	63.546	8.92	384.3	5.9	3.615
139	95.94	10.22	251	2	3.147
147	47.867	4.54	520	0.25	2.951
175	207.2	11.34	127	0.48	4.95
125	58.9331	8.9	421	1.7	2.505
144	196.966	19.3	129.1	4.5	4.0781
154	112.411	8.64	240	1.4	2.979
126	55.845	7.88	449	1	2.866
162	118.71	7.29	217	0.91	5.831
136	98.906	11.49	63	0.5	2.737
137	106.42	12.02	240	1	3.89
134	50.9415	6.11	24.9	0.5	3.024
144	107.868	10.49	235	6.2	4.086
138	65.409	7.133	388	1.7	2.6648
171	204.383	11.85	129	0.67	3.456

Table S12. The adsorption energy and C-H bond activation energy barrier of C_3H_8 and C_3H_6 on Pt-M(111) from ML prediction

Surface	C_3H_8	C_3H_6	Propane to 2-propyl	Propylene to 2-propenyl
Ag-bulk-1:1	-0.562	-1.270	0.954	1.192
Ag-bulk-3:1	-0.553	-1.504	0.802	1.204
Ag-firstlayer-1:1	-0.531	-1.629	0.717	0.985
Ag-firstlayer-3:1	-0.567	-1.571	0.801	1.075
Ag-secondlayer-1:1	-0.587	-1.275	0.890	1.007
Ag-secondlayer-3:1	-0.612	-1.463	0.773	0.876
Au-bulk-1:1	-0.583	-1.397	0.884	1.237
Au-bulk-3:1	-0.600	-1.623	0.791	0.831
Au-first-1:1	-0.513	-1.695	0.794	1.038
Au-first-3:1	-0.577	-1.622	0.773	1.134
Au-second-1:1	-0.576	-1.269	0.883	1.058
Au-second-3:1	-0.605	-1.532	0.852	0.914
Cd-bulk-1:1	-0.448	-1.006	0.984	1.137
Cd-bulk-3:1	-0.503	-0.973	0.950	1.199
Cd-first-1:1	-0.479	-1.409	0.945	1.202
Cd-first-3:1	-0.507	-1.234	0.997	1.176
Cd-second-1:1	-0.579	-1.360	1.026	1.256
Cd-second-3:1	-0.583	-1.488	0.972	1.111
Co-bulk-1:1	-0.495	-1.150	1.084	1.075
Co-bulk-3:1	-0.567	-1.391	0.973	0.889
Co-first-1:1	-0.502	-2.052	0.634	0.897
Co-first-3:1	-0.535	-1.677	0.645	0.770
Co-second-1:1	-0.575	-1.377	0.957	0.948
Co-second-3:1	-0.594	-1.610	0.790	1.015
Cr-bulk-1:1	-0.527	-1.390	0.986	0.972
Cr-bulk-3:1	-0.550	-1.406	0.941	0.978
Cr-first-1:1	-0.505	-1.897	0.643	0.861
Cr-first-3:1	-0.523	-1.729	0.652	0.985
Cr-second-1:1	-0.600	-1.275	0.864	0.926
Cr-second-3:1	-0.586	-1.587	0.794	1.058
Cu-bulk-1:1	-0.619	-1.493	0.863	1.080
Cu-bulk-3:1	-0.584	-1.533	0.879	1.307
Cu-first-1:1	-0.604	-2.039	0.637	0.959
Cu-second-1:1	-0.602	-1.440	0.640	0.983
Cu-second-3:1	-0.648	-1.672	0.913	0.954
Fe-bulk-1:1	-0.540	-1.047	0.763	1.064
Fe-bulk-3:1	-0.605	-0.978	1.000	0.995
Fe-first-1:1	-0.495	-0.598	0.909	0.877
Fe-first-3:1	-0.580	-0.189	0.655	1.056

Fe-second-1:1	-0.584	-0.755	0.628	0.931
Fe-second-3:1	-0.592	-0.395	0.863	0.827
Hf-bulk-1:1	-0.497	-1.095	0.611	0.737
Hf-bulk-3:1	-0.509	-1.052	0.857	1.102
Hf-first-1:1	-0.490	-1.216	0.903	0.962
Hf-first-3:1	-0.528	-0.953	0.795	0.981
Hf-second-1:1	-0.620	-1.274	0.692	1.026
Hf-second-3:1	-0.590	-1.283	0.929	0.917
Hg-bulk-3:1	-0.520	-1.058	0.767	1.241
Hg-first-1:1	-0.503	-1.389	0.865	1.189
Hg-first-3:1	-0.504	-1.170	0.943	1.224
Hg-second-1:1	-0.585	-1.348	0.931	1.214
Hg-second-3:1	-0.588	-1.445	1.043	1.162
Ir-bulk-1:1	-0.509	-1.145	0.811	0.998
Ir-bulk-3:1	-0.534	-1.186	0.835	0.916
Ir-first-1:1	-0.522	-1.843	0.782	1.067
Ir-first-3:1	-0.546	-1.681	0.769	0.806
Ir-second-1:1	-0.594	-1.268	0.593	1.072
Ir-second-3:1	-0.606	-1.560	0.921	0.890
Mn-bulk-1:1	-0.542	-0.886	0.789	1.239
Mn-bulk-3:1	-0.532	-0.939	0.875	1.253
Mn-first-1:1	-0.516	-1.551	0.799	1.059
Mn-first-3:1	-0.513	-1.483	0.701	1.272
Mn-second-1:1	-0.583	-1.132	0.719	1.062
Mn-second-3:1	-0.557	-1.259	0.819	1.084
Mo-bulk-1:1	-0.476	-0.551	0.722	0.590
Mo-bulk-3:1	-0.548	-0.887	0.933	0.851
Mo-first-1:1	-0.573	-1.672	0.844	0.835
Mo-first-3:1	-0.668	-1.589	0.684	1.115
Mo-second-1:1	-0.643	-1.297	0.636	0.898
Mo-second-3:1	-0.662	-1.442	0.873	0.887
Nb-bulk-1:1	-0.472	-0.927	0.716	0.488
Nb-bulk-3:1	-0.497	-0.650	0.954	0.852
Nb-first-1:1	-0.512	-1.681	1.098	0.915
Nb-first-3:1	-0.531	-1.607	0.745	1.174
Nb-second-1:1	-0.630	-1.288	0.674	0.975
Nb-second-3:1	-0.587	-1.442	0.879	0.966
Ni-bulk-1:1	-0.532	-1.391	1.001	0.988
Ni-bulk-3:1	-0.731	-1.734	0.854	1.027
Ni-first-1:1	-0.543	-2.316	0.825	0.960
Ni-first-3:1	-0.713	-1.992	0.675	1.102
Ni-second-1:1	-0.597	-1.527	0.627	1.010
Ni-second-3:1	-0.593	-1.564	0.898	0.871
Os-bulk-1:1	-0.502	-1.185	0.760	0.989

Os-bulk-3:1	-0.536	-1.199	0.961	0.863
Os-first-1:1	-0.504	-1.846	0.881	1.028
Os-first-3:1	-0.536	-1.716	0.818	0.857
Os-second-1:1	-0.605	-1.271	0.625	1.036
Os-second-3:1	-0.590	-1.560	0.917	0.853
Pb-bulk-3:1	-0.442	-0.793	0.837	1.320
Pb-first-1:1	-0.448	-1.040	0.848	1.148
Pb-first-3:1	-0.346	-0.579	0.968	1.243
Pb-second-1:1	-0.526	-1.147	0.966	1.148
Pb-second-3:1	-0.493	-1.061	1.015	0.933
Pd-bulk-1:1	-0.586	-1.576	0.934	0.975
Pd-bulk-3:1	-0.589	-1.659	0.810	1.153
Pd-first-1:1	-0.520	-1.842	0.848	0.815
Pd-first-3:1	-0.597	-1.779	0.656	0.900
Pd-second-1:1	-0.600	-1.207	0.651	0.873
Pd-second-3:1	-0.610	-1.557	0.854	0.908
Re-bulk-1:1	-0.496	-1.042	0.711	0.818
Re-bulk-3:1	-0.513	-1.029	0.982	0.765
Re-first-1:1	-0.514	-1.486	0.893	0.906
Re-first-3:1	-0.527	-1.437	0.746	0.868
Re-second-1:1	-0.609	-1.026	0.607	0.914
Re-second-3:1	-0.601	-1.407	0.877	0.777
Rh-bulk-1:1	-0.514	-1.349	0.762	1.267
Rh-bulk-3:1	-0.539	-1.463	0.960	1.268
Rh-first-1:1	-0.534	-1.830	0.877	1.085
Rh-first-3:1	-0.552	-1.752	0.736	1.070
Rh-second-1:1	-0.590	-1.316	0.764	1.121
Rh-second-3:1	-0.607	-1.532	0.860	0.999
Ru-bulk-1:1	-0.511	-1.184	0.868	1.266
Ru-bulk-3:1	-0.542	-1.422	0.928	0.787
Ru-first-1:1	-0.544	-1.837	0.828	0.878
Ru-first-3:1	-0.539	-1.777	0.711	0.736
Ru-second-1:1	-0.603	-1.323	0.600	0.914
Ru-second-3-1	-0.589	-1.531	0.862	0.850
Sc-bulk-1:1	-0.579	-1.360	0.841	0.899
Sc-bulk-3:1	-0.548	-0.909	0.880	1.229
Sc-first-1:1	-0.486	-1.286	0.912	0.976
Sc-first-3:1	-0.539	-1.210	0.823	1.040
Sc-second-1:1	-0.608	-1.291	0.729	1.039
Sc-second-3:1	-0.576	-1.307	0.913	0.908
Sn-bulk-3:1	-0.564	-1.022	0.802	1.048
Sn-first-1:1	-0.520	-0.892	0.893	1.332
Sn-first-3:1	-0.432	-1.219	0.997	1.386
Sn-second-1:1	-0.557	-1.580	0.852	1.217

Sn-second-3:1	-0.566	-1.208	0.964	0.941
Ta-bulk-1:1	-0.497	-1.176	0.916	0.803
Ta-bulk-3:1	-0.526	-1.141	0.908	1.129
Ta-first-1:1	-0.500	-1.595	0.935	0.938
Ta-first-3:1	-0.535	-1.585	0.836	0.962
Ta-second-1:1	-0.620	-1.188	0.684	0.997
Ta-second-3:1	-0.589	-1.528	0.913	0.905
Tc-bulk-1:1	-0.478	-1.351	0.794	0.794
Tc-bulk-3:1	-0.499	-1.235	1.036	0.903
Tc-first-1:1	-0.529	-1.827	0.920	0.853
Tc-first-3:1	-0.514	-1.683	0.682	0.848
Tc-second-1:1	-0.609	-1.289	0.689	0.941
Tc-second-3:1	-0.602	-1.529	0.862	0.809
Ti-bulk-1:1	-0.739	-1.972	0.727	0.946
Ti-bulk-3:1	-0.548	-1.009	0.659	1.457
Ti-first-1:1	-0.489	-1.195	0.944	0.786
Ti-first-3:1	-0.656	-1.734	0.759	1.125
Ti-second-1:1	-0.610	-1.104	0.690	0.854
Ti-second-3:1	-0.592	-1.471	0.855	0.875
V-bulk-1:1	-0.507	-1.336	0.852	0.476
V-bulk-3:1	-0.514	-1.075	0.753	1.316
V-first-1:1	-0.507	-1.694	0.981	1.008
V-first-3:1	-0.520	-1.738	0.649	1.215
V-second-1:1	-0.633	-1.216	0.693	1.265
V-second-3:1	-0.594	-1.512	0.875	1.117
W-bulk-1:1	-0.457	-1.000	0.836	0.870
W-bulk-3:1	-0.487	-1.006	1.084	0.776
W-first-1:1	-0.537	-1.657	1.083	1.033
W-first-3:1	-0.553	-1.535	0.773	0.935
W-second-1:1	-0.616	-1.215	0.726	1.071
W-second-3:1	-0.610	-1.439	0.870	0.925
Y-bulk-1:1	-0.569	-1.139	0.837	1.122
Y-bulk-3:1	-0.560	-1.029	0.701	1.415
Y-first-1:1	-0.464	-1.149	0.842	1.053
Y-first-3:1	-0.543	-1.043	0.898	1.126
Y-second-1:1	-0.592	-1.214	0.732	1.072
Y-second-3:1	-0.553	-1.203	0.969	0.988
Zn-bulk-1:1	-0.473	-0.989	0.862	1.116
Zn-bulk-3:1	-0.566	-1.062	1.056	1.234
Zn-first-1:1	-0.466	-1.756	0.965	1.133
Zn-first-3:1	-0.537	-1.584	0.672	1.115
Zn-second-1:1	-0.584	-1.256	0.713	1.198
Zn-second-3:1	-0.596	-1.607	0.980	1.014
Zr-bulk-1:1	-0.533	-1.136	0.878	0.804

Zr-bulk-3:1	-0.548	-1.015	0.883	1.074
Zr-first-1:1	-0.504	-1.256	0.862	0.946
Zr-first-3:1	-0.531	-1.124	0.774	1.049
Zr-second-1:1	-0.635	-1.329	0.682	1.032
Zr-second-3:1	-0.590	-1.328	0.922	0.910

Table S13. The RMSE and R^2 score of four ML methods

C_3H_8 adsorption energy				
	RMSE-train	R^2-train	RMSE-test	R^2-test
GBR	0.01	0.98	0.03	0.84
RFR	0.03	0.92	0.12	0.24
KNR	0.06	0.35	0.13	0.25
ABR	0.03	0.84	0.10	0.23
C_3H_6 adsorption energy				
	RMSE-train	R^2-train	RMSE-test	R^2-test
GBR	0.01	0.91	0.07	0.89
RFR	0.01	0.90	0.24	0.22
KNR	0.24	0.35	0.17	0.53
ABR	0.09	0.89	0.18	0.40
C-H bond activation barrier				
	RMSE-train	R^2-train	RMSE-test	R^2-test
GBR	0.03	0.98	0.07	0.82
RFR	0.06	0.90	0.11	0.59
KNR	0.15	0.46	0.12	0.52
ABR	0.09	0.80	0.13	0.43

Table S14. Training features in construction of SISSO model

	R_{E8}	R_{E6}	I_m	N_m	H_{fm}	H_{Vm}	χ
Ga	-0.07	0.37	5.999	1.81	0.058	2.653	0.300
Co	0.46	0.5	7.881	1.88	0.168	3.887	0.660
V	-0.04	0.12	6.746	1.63	0.236	4.695	0.524
Cu	0.05	0.83	7.727	1.9	0.136	3.110	1.227
Zn	0.4	0.56	9.394	1.65	0.076	1.233	0.000
Ag	-0.11	0.5	7.576	1.93	0.117	2.643	1.302

Ru	-0.03	0.08	7.361	2.2	0.266	6.012	1.050
Pd	-0.09	0.35	8.337	2.2	0.173	3.939	0.557
Au	-0.17	0.73	9.225	2.54	0.130	3.421	2.309
Sn	0.07	0.46	7.344	1.96	0.073	3.006	1.112
Nb	0.29	0.64	6.759	1.6	0.278	7.152	0.892
Tc	0.13	0.72	7.280	1.9	0.238	5.701	0.549
Sc	-0.37	0.71	6.562	1.36	0.166	3.296	0.188
Ni	-0.47	0.67	7.640	1.91	0.178	3.918	1.161
Ru	-0.45	0.78	7.361	2.2	0.266	6.012	1.050
Ti	-0.34	0.05	6.828	1.54	0.194	4.405	0.079
Rh	0.58	0.73	7.459	2.28	0.225	5.131	1.137
Hg	0.15	0.55	10.438	2	0.024	0.614	0.000
Pt	-0.32	0.15	9.020	2.28	0.207	5.079	2.128
In	-0.09	0.2	5.786	1.78	0.034	2.384	0.300

	R_{Sm}	R_{Dm}	r_d	e_d	N_{dsm}	ρ	M
Ga	1.058	0.285	1.3	10	12	5.904	69.723
Co	1.32	0.36	1.35	7	9	8.9	58.933
V	1.54	0.48	1.35	3	5	6.11	50.942
Cu	1.37	0.33	1.35	10	11	8.92	63.546
Zn	1.2	0.3	1.35	10	12	7.14	65.380
Ag	1.53	0.55	1.6	10	11	10.49	107.868
Ru	1.65	0.64	1.3	7	8	12.37	101.070
Pd	1.56	0.58	1.4	10	10	12.023	106.420
Au	1.56	0.64	1.35	10	11	19.3	196.966
Sn	1.139	0.468	1.45	10	12	7.31	118.710
Nb	1.82	0.79	1.45	4	5	8.57	92.906
Tc	1.57	0.67	1.35	5	7	11.5	98.000
Sc	1.72	0.59	1.6	1	3	2.985	44.955
Ni	1.28	0.34	1.35	8	10	8.908	58.693
Ru	1.65	0.64	1.3	7	8	12.37	101.070
Ti	1.62	0.53	1.4	2	4	4.507	47.867
Rh	1.6	0.6	1.35	8	9	12.45	102.905
Hg	1.42	0.61	1.5	10	12	13.534	200.590
Pt	1.59	0.66	1.35	9	10	21.09	195.084
In	1.234	0.491	1.55	10	12	7.31	114.818

Table S15. Prediction energy barrier of 4D SISSO model

Surface	Propane to 2-propyl	Propylene to 2-propenyl
Ag-bulk-1:1	0.757	1.246
Ag-bulk-3:1	0.678	1.264
Ag-firstlayer-1:1	0.659	0.978
Ag-firstlayer-3:1	0.677	1.085
Ag-secondlayer-1:1	0.723	1.003
Ag-secondlayer-3:1	0.668	0.868
Au-bulk-1:1	0.681	1.145
Au-bulk-3:1	0.591	0.669
Au-first-1:1	0.594	0.867
Au-first-3:1	0.577	0.991
Au-second-1:1	0.680	0.892
Au-second-3:1	0.652	0.733
Cd-bulk-1:1	0.777	1.222
Cd-bulk-3:1	0.755	1.312
Cd-first-1:1	0.752	1.317
Cd-first-3:1	0.785	1.278
Cd-second-1:1	0.806	1.402
Cd-second-3:1	0.769	1.187
Co-bulk-1:1	0.893	1.058
Co-bulk-3:1	0.797	0.855
Co-first-1:1	0.588	0.863
Co-first-3:1	0.585	0.749
Co-second-1:1	0.781	0.912
Co-second-3:1	0.633	0.986
Cr-bulk-1:1	0.775	0.981
Cr-bulk-3:1	0.750	0.986
Cr-first-1:1	0.698	0.880
Cr-first-3:1	0.696	0.994
Cr-second-1:1	0.732	0.932
Cr-second-3:1	0.705	1.080
Cu-bulk-1:1	0.700	1.061
Cu-bulk-3:1	0.714	1.402
Cu-first-1:1	0.457	0.920
Cu-second-1:1	0.461	0.945
Cu-second-3:1	0.744	0.915
Fe-bulk-1:1	0.653	1.082
Fe-bulk-3:1	0.760	1.000
Fe-first-1:1	0.709	0.879
Fe-first-3:1	0.648	1.072

Fe-second-1:1	0.652	0.932
Fe-second-3:1	0.693	0.848
Ga-bulk-3:1	0.614	0.924
Ga-first-1:1	0.556	0.793
Ga-first-3:1	0.575	1.108
Ga-second-1：1	0.586	0.895
Ga-second-3:1	0.811	0.663
Ge-bulk-3:1	0.591	0.844
Ge-first-1:1	0.588	0.858
Ge-first-3:1	0.465	0.995
Ge-second-1:1	0.465	0.856
Ge-second-3:1	0.489	0.746
Hf-bulk-1:1	0.786	0.642
Hf-bulk-3:1	0.802	1.015
Hf-first-1:1	0.810	0.848
Hf-first-3:1	0.784	0.868
Hf-second-1:1	0.765	0.920
Hf-second-3:1	0.812	0.800
Hg-bulk-3:1	0.641	1.389
Hg-first-1:1	0.690	1.307
Hg-first-3:1	0.746	1.361
Hg-second-1:1	0.736	1.345
Hg-second-3:1	0.828	1.268
In-bulk-3:1	0.756	1.346
In-first-1:1	0.757	1.249
In-first-3:1	0.819	0.858
In-second-1:1	0.755	1.083
In-second-3:1	0.879	0.738
Ir-bulk-1：1	0.725	1.031
Ir-bulk-3：1	0.735	0.970
Ir-first-1:1	0.712	1.112
Ir-first-3:1	0.706	0.841
Ir-second-1:1	0.705	1.119
Ir-second-3:1	0.758	0.920
Mn-bulk-1：1	0.784	1.341
Mn-bulk-3：1	0.817	1.364
Mn-first-1:1	0.787	1.087
Mn-first-3:1	0.776	1.395
Mn-second-1:1	0.776	1.090
Mn-second-3:1	0.796	1.118
Mo-bulk-1:1	0.735	0.551
Mo-bulk-3:1	0.804	0.749
Mo-first-1:1	0.787	0.736
Mo-first-3:1	0.723	1.043

Mo-second-1:1	0.733	0.795
Mo-second-3:1	0.795	0.784
Nb-bulk-1:1	0.646	0.399
Nb-bulk-3:1	0.822	0.658
Nb-first-1:1	0.962	0.729
Nb-first-3:1	0.673	1.033
Nb-second-1:1	0.631	0.782
Nb-second-3:1	0.780	0.772
Ni-bulk-1:1	0.830	0.980
Ni-bulk-3:1	0.694	1.026
Ni-first-1:1	0.666	0.950
Ni-first-3:1	0.562	1.118
Ni-second-1:1	0.553	1.006
Ni-second-3:1	0.733	0.874
Os-bulk-1：1	0.717	0.838
Os-bulk-3：1	0.775	0.709
Os-first-1:1	0.763	0.883
Os-first-3:1	0.743	0.704
Os-second-1:1	0.696	0.892
Os-second-3:1	0.770	0.700
Pb-bulk-3:1	0.637	1.527
Pb-first-1:1	0.642	1.253
Pb-first-3:1	0.696	1.396
Pb-second-1:1	0.695	1.253
Pb-second-3:1	0.726	0.993
Pd-bulk-1:1	0.724	0.945
Pd-bulk-3:1	0.629	1.166
Pd-first-1:1	0.661	0.790
Pd-first-3:1	0.532	0.867
Pd-second-1:1	0.529	0.843
Pd-second-3:1	0.667	0.875
Rh-bulk-1：1	0.581	1.352
Rh-bulk-3：1	0.764	1.355
Rh-first-1:1	0.698	1.085
Rh-first-3:1	0.556	1.067
Rh-second-1:1	0.584	1.132
Rh-second-3:1	0.683	0.982
Ru-bulk-1:1	0.713	1.282
Ru-bulk-3:1	0.773	0.707
Ru-first-1:1	0.668	0.789
Ru-first-3:1	0.525	0.665
Ru-second-1:1	0.448	0.860
Ru-second-3-1	0.706	0.763
Sc-bulk-1：1	0.697	0.736

Sc-bulk-3：1	0.716	1.150
Sc-first-1:1	0.730	0.815
Sc-first-3:1	0.687	0.889
Sc-second-1:1	0.643	0.887
Sc-second-3:1	0.730	0.745
Sn-bulk-3:1	0.622	1.035
Sn-first-1:1	0.683	1.463
Sn-first-3:1	0.775	1.566
Sn-second-1:1	0.656	1.268
Sn-second-3:1	0.743	0.915
Ta-bulk-1：1	0.816	0.428
Ta-bulk-3：1	0.815	0.783
Ta-first-1:1	0.817	0.556
Ta-first-3:1	0.800	0.581
Ta-second-1:1	0.743	0.619
Ta-second-3:1	0.815	0.521
Tc-bulk-1:1	0.674	0.736
Tc-bulk-3:1	0.911	0.845
Tc-first-1:1	0.791	0.788
Tc-first-3:1	0.575	0.784
Tc-second-1:1	0.580	0.874
Tc-second-3:1	0.742	0.748
Ti-bulk-1:1	0.602	0.872
Ti-bulk-3:1	0.570	1.667
Ti-first-1:1	0.769	0.723
Ti-first-3:1	0.620	1.086
Ti-second-1:1	0.583	0.784
Ti-second-3:1	0.707	0.804
V-bulk-1:1	0.723	0.535
V-bulk--3:1	0.619	1.404
V-first-1:1	0.830	0.960
V-first-3:1	0.548	1.237
V-second-1:1	0.573	1.318
V-second-3:1	0.744	1.096
W-bulk-1：1	0.729	0.535
W-bulk-3：1	0.782	0.452
W-first-1:1	0.781	0.708
W-first-3:1	0.705	0.600
W-second-1:1	0.682	0.754
W-second-3:1	0.738	0.589
Y-bulk-1：1	0.755	1.018
Y-bulk-3：1	0.749	1.513
Y-first-1:1	0.756	0.930

Table S16. The identified equation from SISSO models for activation of propane and propene.

	Equation for E_{b8} predicted based on SISSO analysis
1D	$\frac{0.021 \times R_E \times ln\, N_{dsm}}{N_{dsm}} + 0.855$
2D	$\frac{0.187 \times R_E}{r_d \times ln\, r_d} - \frac{0.869 \times (N_m - H_{fm})}{\sqrt[3]{M}} + 0.012$
3D	$\frac{0.44 \times R_E \times N_m}{{r_d}^2} - \frac{0.012 \times (N_m - H_{fm})}{\sqrt[3]{M}} + \frac{0.005 \times N_{dsm} \times \lvert R_E - H_{fm} \rvert}{R_{Dm}} + 0.011$
5D	$\frac{0.184 \times R_E}{r_d \times ln\, r_d} - \frac{0.0198 \times I_m \times {N_m}^3}{\rho} - \frac{0.011 \times {N_m}^3 \times r_d}{M} + \frac{0.018 \times {R_E}^3}{R_{sm} - r_d} + 0.278 \times \lvert {R_E}^2 - {H_{fm}}^2 \rvert + 0.011$
	Equation for E_{b6} predicted based on SISSO analysis
1D	$\frac{0.022 \times ln\, N_m}{N_m - R_E} + 0.086$
2D	$\frac{0.023 \times ln\, N_m}{N_m - R_E} - 0.023 \times \lvert r_d - R_{sm} \rvert^3 + 0.138$
3D	$\frac{0.023 \times ln\, N_m}{N_m - R_E} - \frac{0.00003 \times r_d \times e^{-H_{vm}}}{R_E} - \frac{0.017 \times ln\, R_{Dm}}{H_{fm} - R_E} + 0.094$
5D	$\frac{0.021 \times R_E \times ln\, N_m}{N_m} - \frac{0.716 \times N_{dm} \times \lvert r_d - R_{sm} \rvert}{N_{dsm}} + \frac{0.02 \times \chi}{M \times \lvert R_E - H_{fm} \rvert} - 0.038 \times \lvert \chi^2 - H_{fm} \times H_{vm} \rvert + \frac{0.012 \times ln\, R_E}{\lvert r_d - R_{sm} \rvert} + 0.922$

Table S17. The energy barrier of forward (fwd) and backward (bwd), rate constant, and pre-factor of elementary reaction at 800K on Pt(111). Ads and Des represent adsorption and desorption reactions

	reactions	DFT		Rate constant		Pre-factor	
		fwd	bwd	fwd	bwd	fwd	bwd
Ads	$CH_3CH_2CH_3 + * \rightarrow CH_3CH_2CH_3*$	—	—	1.40×10^{8}	5.92×10^{15}	1.40×10^{8}	1.10×10^{19}
R1	$CH_3CH_2CH_3 + 2* \rightarrow CH_3CH_2CH_2* + H*$	0.93	0.81	2.07×10^{6}	2.36×10^{7}	1.92×10^{13}	1.92×10^{13}
R2	$CH_3CH_2CH_3 + 2* \rightarrow CH_3CHCH_3* + H*$	0.94	0.76	1.53×10^{7}	3.92×10^{9}	1.92×10^{13}	1.92×10^{13}
R3	$CH_3CH_2CH_2* + * \rightarrow CH_3CH_2CH* + H*$	0.96	0.63	8.51×10^{6}	2.33×10^{12}	1.92×10^{13}	1.92×10^{13}
R4	$CH_3CH_2CH_2* + * \rightarrow CH_3CHCH_2* + H*$	0.93	0.85	3.75×10^{9}	1.58×10^{11}	1.92×10^{13}	1.92×10^{13}
R5	$CH_3CHCH_3* + * \rightarrow CH_3CHCH_2* + H*$	0.96	0.99	4.89×10^{5}	3.14×10^{8}	1.92×10^{13}	1.92×10^{13}
R6	$CH_3CHCH_3* + * \rightarrow CH_3CCH_3* + H*$	1.08	0.75	4.59×10^{6}	1.63×10^{12}	1.92×10^{13}	1.92×10^{13}
R9	$CH_3CHCH_2* + * \rightarrow CH_3CHCH* + H*$	0.56	1.08	1.00×10^{5}	9.83×10^{9}	1.92×10^{13}	1.92×10^{13}
R10	$CH_3CHCH_2* + * \rightarrow CH_3CCH_2* + H*$	1.04	0.76	5.05×10^{4}	4.28×10^{10}	1.92×10^{13}	1.92×10^{13}
R11	$CH_3CCH_3* + * \rightarrow CH_3CCH_2* + H*$	1.09	0.89	4.13×10^{6}	2.66×10^{8}	1.92×10^{13}	1.92×10^{13}
R13	$CH_3CHCH* + * \rightarrow CH_3CHC* + H*$	0.83	0.93	8.02×10^{6}	1.39×10^{9}	1.92×10^{13}	1.92×10^{13}
R14	$CH_3CHCH* + * \rightarrow CH_3CCH* + H*$	1.38	1.19	8.58×10^{9}	6.75×10^{9}	1.92×10^{13}	1.92×10^{13}
R15	$CH_3CCH_2* + * \rightarrow CH_3CCH* + H*$	1.07	0.88	3.04×10^{9}	3.22×10^{10}	1.92×10^{13}	1.92×10^{13}
R16	$CH_3CHC* + * \rightarrow CH_3CC* + H*$	1.15	0.78	3.72×10^{6}	1.25×10^{10}	1.92×10^{13}	1.92×10^{13}
R17	$CH_3CCH* + * \rightarrow CH_3CC* + H*$	1.53	0.44	7.27×10^{3}	2.08×10^{9}	1.92×10^{13}	1.92×10^{13}
R23	$CH_3CCH_3* + * \rightarrow CH_3* + CH_3C*$	1.68	0.59	2.86×10^{3}	9.09×10^{4}	1.92×10^{13}	1.92×10^{13}
R26	$CH_3CCH_2* + * \rightarrow CH_2* + CH_3C*$	1.45	1.77	2.62×10^{1}	3.49×10^{8}	1.92×10^{13}	1.92×10^{13}
R28	$CH_3CCH* + * \rightarrow CH* + CH_3C*$	1.78	1.73	1.47×10^{3}	2.37×10^{6}	1.92×10^{13}	1.92×10^{13}

H_2	$H^* + H^* \rightarrow H_2^* + *$	1.45	1.69	3.60×10^{7}	6.15×10^{10}	1.92×10^{13}	1.92×10^{13}
Des	$CH_3CHCH_2^* \rightarrow CH_3CHCH_2 + *$	—	—	1.43×10^{8}	2.80×10^{11}	1.43×10^{8}	7.01×10^{18}
Des	$H_2^* \rightarrow H_2 + *$	—	—	6.58×10^{8}	9.02×10^{14}	6.58×10^{8}	4.11×10^{15}

Table S18. The energy barrier of forward (fwd) and backward (bwd), rate constant, and pre-factor of elementary reaction at 800K on $Pt_3Mo(111)$. Ads and Des represent adsorption and desorption reactions

reactions		DFT		Rate constant		Pre-factor	
		fwd	bwd	fwd	bwd	fwd	bwd
Ads	$CH_3CH_2CH_3 + * \rightarrow CH_3CH_2CH_3^*$	—	—	1.40×10^{8}	5.28×10^{15}	1.40×10^{8}	1.10×10^{19}
R1	$CH_3CH_2CH_3 + 2\,* \rightarrow CH_3CH_2CH_2^* + H^*$	0.64	0.71	3.71×10^{7}	3.15×10^{6}	1.92×10^{13}	1.92×10^{13}
R2	$CH_3CH_2CH_3 + 2\,* \rightarrow CH_3CHCH_3^* + H^*$	0.67	0.73	8.64×10^{6}	2.03×10^{8}	1.92×10^{13}	1.92×10^{13}
R3	$CH_3CH_2CH_2^* + * \rightarrow CH_3CH_2CH^* + H^*$	0.99	0.65	6.41×10^{5}	2.81×10^{10}	1.92×10^{13}	1.92×10^{13}
R4	$CH_3CH_2CH_2^* + * \rightarrow CH_3CHCH_2^* + H^*$	0.64	0.73	7.06×10^{9}	1.66×10^{9}	1.92×10^{13}	1.92×10^{13}
R5	$CH_3CHCH_3^* + * \rightarrow CH_3CHCH_2^* + H^*$	0.67	0.88	2.92×10^{6}	8.64×10^{6}	1.92×10^{13}	1.92×10^{13}
R6	$CH_3CHCH_3^* + * \rightarrow CH_3CCH_3^* + H^*$	1.21	0.67	1.86×10^{13}	1.21×10^{9}	1.92×10^{13}	1.92×10^{13}
R9	$CH_3CHCH_2^* + * \rightarrow CH_3CHCH^* + H^*$	1.10	0.58	1.64×10^{9}	4.30×10^{9}	1.92×10^{13}	1.92×10^{13}
R10	$CH_3CHCH_2^* + * \rightarrow CH_3CCH_2^* + H^*$	1.12	1.15	1.86×10^{6}	1.10×10^{6}	1.92×10^{13}	1.92×10^{13}
R11	$CH_3CCH_3^* + * \rightarrow CH_3CCH_2^* + H^*$	1.18	0.88	3.86×10^{10}	8.37×10^{8}	1.92×10^{13}	1.92×10^{13}
R13	$CH_3CHCH^* + * \rightarrow CH_3CHC^* + H^*$	1.01	0.67	4.02×10^{11}	1.21×10^{10}	1.92×10^{13}	1.92×10^{13}
R14	$CH_3CHCH^* + * \rightarrow CH_3CCH^* + H^*$	1.58	1.29	1.36×10^{10}	1.03×10^{8}	1.92×10^{13}	1.92×10^{13}
R15	$CH_3CCH_2^* + * \rightarrow CH_3CCH^* + H^*$	1.31	0.93	1.36×10^{10}	1.04×10^{9}	1.92×10^{13}	1.92×10^{13}
R16	$CH_3CHC^* + * \rightarrow CH_3CC^* + H^*$	1.34	0.87	2.14×10^{5}	6.56×10^{8}	1.92×10^{13}	1.92×10^{13}
R17	$CH_3CCH^* + * \rightarrow CH_3CC^* + H^*$	1.51	0.63	7.66×10^{6}	2.77×10^{10}	1.92×10^{13}	1.92×10^{13}
R23	$CH_3CCH_3^* + * \rightarrow CH_3^* + CH_3C^*$	1.67	1.33	7.80×10^{5}	2.58×10^{1}	1.92×10^{13}	1.92×10^{13}
R26	$CH_3CCH_2^* + * \rightarrow CH_2^* + CH_3C^*$	1.89	0.75	1.12×10^{5}	3.91×10^{11}	1.92×10^{13}	1.92×10^{13}
R28	$CH_3CCH^* + * \rightarrow CH^* + CH_3C^*$	2.60	1.10	3.69×10^{9}	1.72×10^{7}	1.92×10^{13}	1.92×10^{13}
H_2	$H^* + H^* \rightarrow H_2^* + *$	0.91	0.39	6.88×10^{7}	7.69×10^{11}	1.92×10^{13}	1.92×10^{13}
Des	$CH_3CHCH_2^* \rightarrow CH_3CHCH_2 + *$	—	—	1.43×10^{8}	1.21×10^{15}	1.43×10^{8}	7.01×10^{18}
Des	$H_2^* \rightarrow H_2 + *$	—	—	6.58×10^{8}	1.28×10^{14}	6.58×10^{8}	4.11×10^{15}

References:

1. Nykänen, L.; Honkala, K., Density Functional Theory Study on Propane and Propene Adsorption on Pt(111) and Ptsn Alloy Surfaces. *J. Phys. Chem. C* **2011**, *115*, 9578-9586.
2. Lian, Z.; Ali, S.; Liu, T.; Si, C.; Li, B.; Su, D. S., Revealing the Janus Character of the Coke Precursor in the Propane Direct Dehydrogenation on Pt Catalysts from a Kmc Simulation. *ACS Catal.* **2018**, *8*, 4694-4704.
3. Yang, M.-L.; Zhu, Y.-A.; Zhou, X.-G.; Sui, Z.-J.; Chen, D., First-Principles Calculations of Propane Dehydrogenation over Ptsn Catalysts. *ACS Catal.* **2012**, *2*, 1247-1258.
4. Xiao, L.; Ma, F.; Zhu, Y. A.; Sui, Z. J.; Zhou, J. H.; Zhou, X. G.; Chen, D.; Yuan, W. K., Improved

Selectivity and Coke Resistance of Core-Shell Alloy Catalysts for Propane Dehydrogenation from First Principles and Microkinetic Analysis. *Chem. Eng. J.* **2019**, *377*, 1-37.
5. Zha, S.; Sun, G.; Wu, T.; Zhao, J.; Zhao, Z. J.; Gong, J., Identification of Pt-Based Catalysts for Propane Dehydrogenation Via a Probability Analysis. *Chem Sci* **2018**, *9*, 3925-3931.
6. Terzieff, P.; Komarek, K. L.; Wachtel, E., Magnetic-Properties of Liquid Au-in and Au-Ge Alloys. *Zeitschrift Fur Physikalische Chemie Neue Folge* **1988**, *156*, 563-567.
7. Yang, M.-L.; Zhu, Y.-A.; Fan, C.; Sui, Z.-J.; Chen, D.; Zhou, X.-G., Density Functional Study of the Chemisorption of C1, C2 and C3 Intermediates in Propane Dissociation on Pt(111). *J. Mol. Catal. A: Chem.* **2010**, *321*, 42-49.
8. Hook, A.; Celik, F. E., Predicting Selectivity for Ethane Dehydrogenation and Coke Formation Pathways over Model Pt-M Surface Alloys with Ab Initio and Scaling Methods. *J. Phys. Chem. C* **2017**, *121*, 17882-17892.
9. Wang, T.; Cui, X.; Winther, K. T.; Abild-Pedersen, F.; Bligaard, T.; Nørskov, J. K., Theory-Aided Discovery of Metallic Catalysts for Selective Propane Dehydrogenation to Propylene. *ACS Catal.* **2021**, *11*, 6290-6297.
10. Xiao, L.; Hu, P.; Sui, Z. J.; Chen, D.; Zhou, X. G.; Yuan, W. K.; Zhu, Y. A., Rational Design of Intermetallic Compound Catalysts for Propane Dehydrogenation from a Descriptor-Based Microkinetic Analysis. *J. Catal.* **2021**, *404*, 32-45.